The Astronomical Journal, 138:1667–1680, 2009 December doi:10.1088/0004-6256/138/6/1667

A *HUBBLE SPACE TELESCOPE*/WFPC2 SURVEY OF BRIGHT YOUNG CLUSTERS IN M31. III. STRUCTURAL PARAMETERS*

P. Barmby[1], S. Perina[2,3], M. Bellazzini[2,3], J. G. Cohen[4], P. W. Hodge[5], J. P. Huchra[6], M. Kissler-Patig[7], T. H. Puzia[8], and J. Strader[6,9]

[1] Department of Physics & Astronomy, University of Western Ontario, London, ON N6A 3K7, Canada; pbarmby@uwo.ca
[2] INAF-Osservatorio Astronomico di Bologna, via Ranzani 1, 40127 Bologna, Italy
[3] Università di Bologna, Dipartimento di Astronomia, via Ranzani 1, 40127 Bologna, Italy
[4] Palomar Observatory, Mail Stop 105-24, California Institute of Technology, Pasadena, CA 91125, USA
[5] Department of Astronomy, University of Washington, Seattle, WA 98195, USA
[6] Harvard-Smithsonian Center for Astrophysics, Cambridge, MA 02138, USA
[7] European Southern Observatory, Karl-Schwarzschild-Strasse 2, 85748 Garching bei München, Germany
[8] Herzberg Institute of Astrophysics, 5071 West Saanich Road, Victoria, BC V9E 2E7, Canada
Received 2009 July 31; accepted 2009 September 15; published 2009 October 30

ABSTRACT

Surface brightness profiles for 23 M31 star clusters were measured using images from the Wide Field Planetary Camera 2 on the *Hubble Space Telescope*, and fitted to two types of models to determine the clusters' structural properties. The clusters are primarily young ($\sim 10^8$ yr) and massive ($\sim 10^{4.5}$ $M_\odot$), with median half-light radius 7 pc and dissolution times of a few Gyr. The properties of the M31 clusters are comparable to those of clusters of similar age in the Magellanic Clouds. Simulated star clusters are used to derive a conversion from statistical measures of cluster size to half-light radius so that the extragalactic clusters can be compared to young massive clusters in the Milky Way. All three sets of star clusters fall approximately on the same age–size relation. The young M31 clusters are expected to dissolve within a few Gyr and will not survive to become old, globular clusters. However, they do appear to follow the same fundamental plane (FP) relations as old clusters; if confirmed with velocity dispersion measurements, this would be a strong indication that the star cluster FP reflects universal cluster formation conditions.

Key words: galaxies: individual (Messier: Number M31) – galaxies: star clusters – globular clusters: general

Online-only material: machine-readable and VO tables

1. INTRODUCTION

The spatial distribution of stars within a star cluster is an important indicator of the cluster's dynamical state, and the structural parameters (e.g., core, half-light, and tidal radii; central surface brightness and concentration) indicate on what timescales the cluster is "bound" to dissolve. The work of Spitzer (1987) showed that core collapse is an inevitable part of cluster dynamical evolution. Djorgovski & King (1986) were among the first to determine the fraction of core-collapsed Milky Way globular clusters (GCs), while Djorgovski & Meylan (1994) examined a large sample of Milky Way clusters and defined the "fundamental plane (FP)," showing that surface brightness profiles of Galactic GCs were well described by only a few parameters. Meylan & Djorgovski (1987) surveyed GCs in the LMC and SMC for core collapse and found that only a handful of clusters were core-collapse candidates; they suggested that environmental or age effects were responsible for the difference with Milky Way globulars.

A few spatially resolved studies of GCs beyond the Magellanic Clouds (MCs) were done with ground-based data. Racine (1991) and Racine & Harris (1992) used high-resolution imaging to distinguish M31 GC candidates from background galaxies, and Cohen & Freeman (1991) determined the tidal radii of 30 M31 halo GCs, finding them to be similar to Milky Way GCs. However, detailed studies of the structures of M31 GCs awaited the angular resolution of the *Hubble Space Telescope* (*HST*). The first work on M31 GCs by Bendinelli et al. (1993) and Fusi Pecci et al. (1994) was followed by numerous others including Rich et al. (1996), Grillmair et al. (1996), Holland et al. (1997), and Barmby et al. (2002, 2007). Clusters in Local Group galaxies are near the limit for resolution into individual stars by the *HST*, although some structural information such as half-light radii can be recovered for clusters in more distant galaxies (e.g., Haşegan et al. 2005). Conclusions of the studies of extragalactic globulars include the dependence of cluster size on galactocentric radius, first pointed out for the Milky Way by Djorgovski & Meylan (1994) and van den Bergh (1994); a possible difference between sizes of clusters in different metallicity groups (for a detailed discussion, see Jordán 2004); and a recognition that GCs in a variety of environments appear to lie on the same FP (Barmby et al. 2007).

Structural studies of younger star clusters present more difficulties. Open clusters (OCs) in the Milky Way are generally much less massive than GCs. As viewed from our location in the Milky Way, they are embedded within the disk, so that the cluster is easily lost against the much more numerous field stars, and determining stellar membership in these less-concentrated objects is not straightforward. Comprehensive studies of Milky Way OCs are relatively recent: Kharchenko et al. (2005) and follow-up work (Schilbach et al. 2006; Piskunov et al. 2007, 2008) measured a variety of radii (core, corona, and tidal) for several hundred clusters and found their masses to be in the range 50–1000 $M_\odot$. Bonatto & Bica (2005) analyzed in more detail a much smaller number of Milky Way OCs, finding that the cluster size increased with both age and Galactocentric distance.

* Based on observations made with the NASA/ESA *Hubble Space Telescope*, obtained at the Space Telescope Science Institute, which is operated by the Association of Universities for Research in Astronomy, Inc., under NASA contract NAS 5-26555. These observations are associated with program GO-10818 (PI: J. Cohen) and GO-8296 (PI: P. Hodge).
[9] Hubble Fellow

These authors also found that their sample of clusters showed evidence for an "open cluster fundamental plane."

Milky Way OCs are not the only known population of young star clusters, and possibly not even the best one to study. The Galactic OCs cover a limited range in age and mass and their census is suspected to be far from complete because of extinction in the Galactic plane. The MCs have many young star clusters, recently cataloged by Bica et al. (2008). The brighter MC clusters were studied in a pioneering work by Elson et al. (1987). These authors analyzed the radial profiles of 10 clusters and found them to be better fitted by "power-law" profiles of the form $I(R) \propto [1 + (R/r_0)^2]^{-(\gamma-1)/2}$ than by the King (1966) models conventionally used to fit GC profiles. McLaughlin & van der Marel (2005) re-analyzed a large set of MC cluster data and found the situation to be somewhat more complex. Those authors argued that the extended envelopes characteristic of the power-law profiles are a generic feature of many young *and old* star clusters and that "the development of a physically motivated model accounting for this. . .could lend substantial new insight into questions of cluster formation and evolution."

Outside the Milky Way, many galaxies are found to have "young massive clusters" (YMCs; Holtzman et al. 1992; Whitmore & Schweizer 1995). These clusters have ages up to a few Gyr (Brodie et al. 1998) and masses comparable to GCs (Larsen & Richtler 1999). Studies of YMC structures show correlations of power-law slope γ with age (Larsen 2004), core radius with age (Mackey & Gilmore 2003), and mass of the brightest cluster with galaxy star formation rate (Weidner et al. 2004). As of yet there is no comprehensive study of star cluster structures over the full age and mass ranges seen in nearby galaxies. M31 is now recognized to also have a large population of young star clusters (Fusi Pecci et al. 2005; Caldwell et al. 2009), although their relationship to both the YMCs and GCs is not well understood. The purpose of this paper is to carry out an initial study of the structural properties of some young M31 clusters. We analyze a sample of 23 clusters using data from the Wide Field Planetary Camera 2 (WFPC2) on board the *HST*; extensive analysis of "artificial clusters" (see the Appendix) informs our analysis procedures. Throughout this work, we assume a distance to M31 of 783 kpc (Stanek & Garnavich 1998), for which 1″ corresponds to 3.797 pc. All magnitudes are in the Vega system, and cluster names use the convention of the Revised Bologna Catalog (Galleti et al. 2004);[10] see that work for cluster coordinates and other properties.

2. DATA AND ANALYSIS METHODS

2.1. Cluster Sample

The study of star clusters in M31 has a long history dating back to at least Hubble (1932), so any attempt to assemble a sample of YMCs necessarily draws on many previous works. While a number of studies of the GC system have noted the presence of possible young clusters in M31 (Barmby et al. 2000; Williams & Hodge 2001), the first comprehensive list of such objects was assembled by Fusi Pecci et al. (2005), who called them "blue luminous compact clusters," or BLCCs. Krienke & Hodge (2007, 2008) and Hodge et al. (2009) searched for M31 "disk clusters" in archival *HST* imaging data, and Caldwell et al. (2009) presented a comprehensive list of nearly 150 young cluster candidates from a spectroscopic survey. Caldwell et al. (2009) noted that the handful of their young clusters with measured structural properties (from Barmby et al. 2007) covered a wide range in parameter space. The *HST*-resolved star study of four "massive and compact young star clusters" by Williams & Hodge (2001; program GO-8296) did not include an analysis of the objects' structural properties.

The main sample of clusters studied here is described in detail by the companion papers by Perina et al. (2009a, 2009b). The present project began with an interest in confirming the results of Cohen et al. (2005) who used adaptive optics imaging to show that some of the clusters proposed as young were in fact asterisms (but see the contrary view of Caldwell et al. 2009 and the discussion in Perina et al. 2009a). *HST* program GO-10818 was aimed at imaging all of the "class A" clusters proposed by Fusi Pecci et al. (2005) which did not already have *HST* imaging, a total of 21 objects. In the course of the program, we found that two clusters in the candidate list were in fact the same object (Perina et al. 2009a), and the object NB67 was a star, so the program contains 19 objects. Perina et al. (2009b) showed that 16 of the clusters are young, with ages <1 Gyr, and five (B083, B222, B347, B374, and NB16) are in fact intermediate aged or old (see also Caldwell et al. 2009). We retain these five clusters in our sample but show them with different symbols in the analysis. We augmented the GO-10818 data with archival data on the four clusters studied by Williams & Hodge (2001) to bring the total number of clusters to 23. *HST* archival data exist for additional clusters but in the interests of dealing with a mostly homogeneous data set we restricted the sample to only the GO-10818 and GO-8296 clusters. Three of the clusters in the latter data set had structural parameters reported in Barmby et al. (2002); here we re-analyze them in a manner consistent with the other clusters. Except for B083 and B347, all of the clusters are projected against the M31 disk (see Figure 1 of Perina et al. 2009b).

2.2. Data Reduction and Surface Brightness Profiles

The GO-10818 program was originally intended to be carried out with the Advanced Camera for Surveys (ACS), but because that instrument failed, the images were obtained instead with the WFPC2. All objects were observed with two 400 s dithered images in each of two filters: F450W and F814W (for further detail, and an example of the color–magnitude diagram (CMD) analysis, see Perina et al. 2009a). The GO-8296 program was also carried out with WFPC2 and involved two 800 s images in F439W and two 600 s images in F555W (as well as longer images in F336W which are not used here). The target clusters were on the Planetary Camera (PC) chip in all cases, and only data from that chip are used in the present analysis. Table 1 summarizes the data sets together with other pertinent information about the clusters.

The multiple images were combined with the STScI Multidrizzle software, using the "recipes" provided on the drizzle webpage. The pixel scale of the resulting images was 0.″0455, or 0.172 pc at the M31 distance. While correcting for charge transfer efficiency losses would be desirable, there is currently no prescription available for correcting surface photometry of extended objects so no correction has been made in the present analysis. Although M31 star clusters are relatively large (a few arcsec) compared to the *HST* optical point-spread function (PSF), convolving model profiles with the PSF prior to comparison with the data should improve the accuracy of measurements of the cluster cores. Model PSFs were generated for the relevant filters at the camera center using TinyTim. The clusters are small compared to the camera

[10] Online version at http://www.bo.astro.it/M31.

Table 1
Data for M31 Young Clusters

Name[a]	Data Set 1	Data Set 2	Filter 1	Exposure 1 (s)	Filter 2	Exposure 2 (s)	$E(B-V)$	log Age (yr)
B015D	u9pi140[12]	u9pi140[34]	F450W	800	F814W	800	0.65	7.85
B040	u9pi050[12]	u9pi050[34]	F450W	800	F814W	800	0.23	7.90
B043	u9pi022[12]	u9pi022[34]	F450W	800	F814W	800	0.23	7.90
B066	u9pi240[12]	u9pi240[34]	F450W	800	F814W	800	0.23	7.85
B081	u9pi170[12]	u9pi170[34]	F450W	800	F814W	800	0.30	8.15
B083	u9pi250[12]	u9pi250[34]	F450W	800	F814W	800	0.20	10.11
B222	u9pi180[12]	u9pi180[34]	F450W	800	F814W	800	0.20	10.11
B257D	u9pi100[12]	u9pi100[34]	F450W	800	F814W	800	0.30	7.90
B315	u5bj010[12]	u5bj010[78]	F439W	1600	F555W	1200	0.31	8.00
B318	u9pi020[12]	u9pi020[34]	F450W	800	F814W	800	0.17	7.85
B319	u5bj020[12]	u5bj020[78]	F439W	1600	F555W	1200	0.23	8.00
B321	u9pi150[12]	u9pi150[34]	F450W	800	F814W	800	0.25	8.23
B327	u9pi030[12]	u9pi030[34]	F450W	800	F814W	800	0.20	7.70
B342	u5bj030[12]	u5bj030[78]	F439W	1600	F555W	1200	0.20	8.20
B347	u9pi230[12]	u9pi230[34]	F450W	800	F814W	800	0.06	10.11
B368	u5bj040[12]	u5bj040[78]	F439W	1600	F555W	1200	0.20	7.80
B374	u9pi070[12]	u9pi070[34]	F450W	800	F814W	800	0.30	10.11
B376	u9pi080[12]	u9pi080[34]	F450W	800	F814W	800	0.30	8.00
B448	u9pi200[12]	u9pi200[34]	F450W	800	F814W	800	0.35	7.90
B475	u9pi090[12]	u9pi090[34]	F450W	800	F814W	800	0.35	8.30
NB16	u9pi120[12]	u9pi012[34]	F450W	800	F814W	800	0.25	10.11
V031	u9pi130[12]	u9pi130[34]	F450W	800	F814W	800	0.35	8.45
VDB0	u9pi010[12]	u9pi010[34]	F450W	800	F814W	800	0.20	7.40

Note. [a] Naming convention of the Revised Bologna Catalog (Galleti et al. 2004) is used. See that work for coordinates.

Table 2
Calibration Data for WFPC2 Imaging

Filter	Zero Point	$M_\odot$	Conversion Factor[a]
F439W	22.987	5.55	45.138
F450W	23.996	5.31	14.274
F555W	24.621	4.83	5.163
F814W	23.641	4.14	6.744

Note. [a] Multiplicative conversion between surface brightness in counts s^{-1} arcsec^{-2} and intensity in $L_\odot$ pc^{-2}.

field of view, and PSF variation over the cluster extent is negligible.

Transforming instrumental magnitudes to calibrated surface brightness was done following the prescription in Barmby et al. (2007). Image counts were first multiplied by the inverse square of the pixel scale to give counts C in units of s^{-1} arcsec^{-2}. These can be transformed to magnitudes arcsec^{-2} through $\mu = Z - 2.5\log(C)$, where Z is the instrument zero point. They can also be transformed to intensity I in $L_\odot$ pc^{-2} through $I = 10^{0.4(Z'-Z)}C$. (Independent of the instrument used, $Z' = (m - M)_{\rm M31} + M_\odot + 5\log(\beta) = 21.5715 + M_\odot$, where β is the number of arcsec corresponding to 1 pc; $\beta = 0.2644$ at the assumed distance of M31.) The zero points used come from the respective instrument handbooks; the solar magnitudes are from calculations by C. Willmer.[11] All are listed in Table 2 for reference.

Studies of surface brightness profiles of Local Group star clusters are in a somewhat different regime from either Galactic clusters or clusters in more distant galaxies. Local Group star clusters are resolved into stars in their outer regions but not in their cores. They differ from galaxies with comparable angular sizes ($\lesssim$10 arcsec for M31 and M33 clusters) in that the galaxies are composed of many more stars and have much smoother light distributions. To better understand the limitations of our analysis, we simulated artificial star clusters, measured their surface brightness profiles, and fit those profiles to models: these simulations are described in the Appendix.

Surface brightness profiles for the M31 clusters were measured by combining integrated photometry with star number counts (the "hybrid" procedure described in the Appendix). In the inner regions of the clusters, surface brightness profiles were derived using the IRAF ELLIPSE package to fit circular isophotes to the image data. The isophote centers were fixed at a single value for each cluster, with centers determined as the intensity-weighted centroid in a 75 × 75 pixel box. Star counts were derived only from stars within specified regions of the CMD, with the designated region varying by cluster depending on the age. The details of the star counts for the GO-10818 clusters are given by Perina et al. (2009b); for the GO-8296 clusters, star counts were computed from background-subtracted CMDs (Figure 6 of Williams & Hodge 2001) with positional data kindly provided by B. Williams. The star counts were used for radii >7 pc (40 pixels) from the cluster centers, and scaled to linear intensity units ($L_\odot$ pc^{-2}) by matching the counts and photometry over the overlap region 5–10 pc. The same star counts were matched to integrated photometry profiles in both red and blue filters, but with different scaling factors; star count uncertainties were matched to the photometry uncertainties by scaling as for the intensity. No background subtraction was performed on the star counts.

2.3. Profile-fitting Methods

There are a number of possible choices for star cluster density profiles, including King (1966, hereafter King), Wilson (1975, hereafter Wilson), King (1962), Elson et al. (1987, also known as "power law" or "EFF"), and Sérsic (1968). Unlike the other three types of model profile, the King and

[11] http://www.ucolick.org/~cnaw/sun.html

Wilson models have no analytic expressions for density or surface brightness as a function of projected radius; profiles are obtained by integrating phase-space distribution functions over all velocities and then along the line of sight, assuming spherical symmetry (for a review, see McLaughlin 2003). The King model is the most commonly used in studies of star clusters; however, McLaughlin & van der Marel (2005) showed that, with data that extend to sufficiently large projected radii, many Local Group clusters are better fitted by the more extended Wilson models. Globulars in NGC 5128 are also better fitted by Wilson models (McLaughlin et al. 2008), although an analysis using nearly identical techniques (Barmby et al. 2007) found that massive M31 globulars were better fitted by King models. Taken together, these recent analyses showed that fitting the King (1962), Elson et al. (1987), and Sérsic (1968) models did not add significant information beyond that provided by the King and Wilson models, so we consider only these two models in our analysis.

The King and Wilson models are single-stellar-mass, isotropic models defined by phase-space distribution functions of stellar energy E:

$$f(E) \propto \begin{cases} \exp[-E/\sigma_0^2] - 1 & , \ E < 0 \quad \text{(King)} \\ \exp[-E/\sigma_0^2] - 1 + E/\sigma_0^2 & , \ E < 0 \quad \text{(Wilson)} \\ 0 & , \ E \geqslant 0 \quad \text{(both)}, \end{cases} \tag{1}$$

where σ_0 is the central velocity dispersion. The effect of the extra term in the Wilson model $f(E)$ is to make clusters more spatially extended. Both sets of models are characterized by three parameters: a dimensionless central potential W_0, which measures the degree of central concentration; a scale radius r_0, which sets the physical scale; and a central intensity I_0, which sets the overall normalization. For the King models, W_0 has a one-to-one correspondence with the more-familiar concentration $c = \log(r_t/r_0)$, where r_t is the tidal radius at which the density $\rho(r_t) = 0$. Possibly contrary to intuitive expectations, for two profiles with the same scale radius, the profile with a larger value of c or W_0 declines more slowly.

Deriving the structural properties of the simulated clusters involved fitting their projected surface density profiles to models using the GRIDFIT program described by McLaughlin & van der Marel (2005; see also McLaughlin et al. 2008). The program uses a grid of model density profiles, precomputed for a range of values of W_0, then finds the scale radius r_0 and central surface brightness I_0 to minimize the weighted χ^2 for each W_0; the best-fitting model is the one with the global χ^2 minimum. The model profiles are convolved with the instrumental PSF before comparison to the data. Since no background subtraction was performed on the star counts, the background level was determined as one of the parameters of the model fitting. For a few clusters, the fitting algorithm converged to unreasonably large or small values, and a fixed background corresponding to the lowest level reached by the star counts was subtracted before re-fitting; in general this procedure improved the reduced χ^2 of the fits.

2.4. Profile-fitting: Results

Figure 1 shows the cluster surface brightness profiles together with the best-fitting models. The parameters of the models are given in Table 3, corrected for extinction using the values of $E(B-V)$ given by Perina et al. (2009b) or Williams & Hodge (2001). Conversion of filter-specific measurements to the V band is done using the transformations described in the appropriate *HST* Instrument Handbooks; briefly, we compute the extinction-corrected color $(V-x)_0$, where x is the observed band magnitude, as a function of color in standard bands (e.g., $(V-I)_0$). Ground-based integrated colors from Galleti et al. (2007) are used for the standard-band colors, to avoid iteration; uncertainties of 0.1 mag in $(V-x)_0$ are assumed and propagated through the parameter estimates. As previously shown by McLaughlin & van der Marel (2005), differences between Wilson and King model profiles occur primarily in the outer parts of cluster profiles, where our signal to noise is low. The similarity between model profiles also means that, in general, the best-fit models of the two families have very similar χ^2, with no strong systematic preference for one model or the other. Typical χ^2 values are 85–90; with ∼20 data points and 3 or 4 model degrees of freedom, the resulting reduced values are $\chi^2_\nu \sim 6$. This indicates that the uncertainties produced by integrated photometry are likely underestimates, and one reason may be that these uncertainties do not account for the uncertainty in the background level. Rather than modifying the uncertainties to achieve $\chi^2_\nu \sim 1$, we modified our use of χ^2 in computing parameter uncertainties (see also McLaughlin et al. 2008). We scaled the reduced χ^2 values such that the best-fit model had $\chi^2_\nu \equiv 1$. The 68% confidence limits on the parameters are then the minimum and maximum values found in the set of models with $\chi^2_\nu \leqslant 2$. This rescaling gives more realistic estimates of the parameter uncertainties than would otherwise be the case.

How robust are the physical parameters derived from our model fits? One way to estimate this is to compare various fits to the same cluster. Although W_0 and r_0 have slightly different meanings in King and Wilson models and cannot be directly compared, some derived quantities such as the half-light radius and total luminosity are directly comparable. For all clusters, we have profile data in two different bandpasses, although the outer parts of the profile, derived from number counts, are the same in both. There are physical reasons why profiles might change with wavelength (e.g., mass segregation and differential reddening), but comparison of model fits in different filters is a useful sanity check. Figure 2 shows this comparison: the scatter between filters is 0.2–0.3 dex. A similar comparison between fits for M31 GCs by Barmby et al. (2007) found a much smaller scatter, probably because that work analyzed bright clusters, using much deeper data. Figure 2 also compares R_h and L_V between Wilson and King models. The scatter is again rather large, 0.15–0.25 dex, with the Wilson models offset to larger values. To some extent this is to be expected, since Wilson models have larger halos; however, some of the Wilson model values (e.g., $R_h > 50$ pc for B015D, B257D, B321, B376, and B448) are physically implausible, because the model fitting resulted in very large values of the central potential W_0. We do not completely understand the reason for this but speculate that it may be related to the combination of the additional power in the haloes of Wilson models and the low signal to noise of the profiles in the same region. These results indicate the limitations of our relatively shallow data, and the limited precision of the model measurements will need to be kept in mind during the following analysis.

For the analysis in the remainder of this paper, we use only a single set of model parameters per cluster. Because the King models have fewer implausible values, and also somewhat less scatter between filters, we use the King model parameters for the present cluster sample. Our results in the Appendix indicate that King model fits may be more robust than Wilson model fits in the case where background levels are uncertain, even where

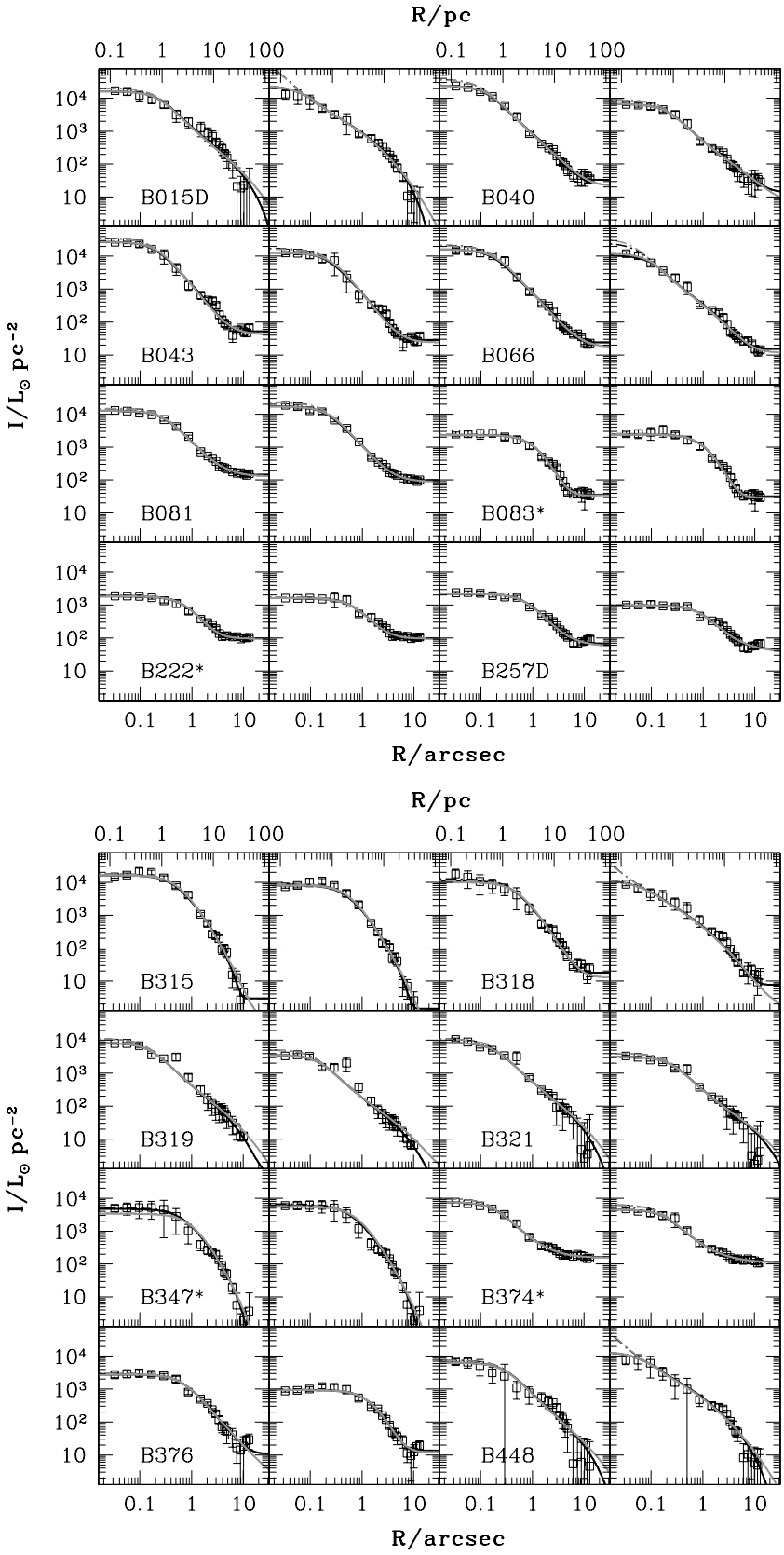

Figure 1. M31 cluster surface brightness profiles together with the best-fitting models. Each cluster is shown in two subpanels, with the bluer filter (F439W or F450W) on the left and the redder filter (F555W or F814W) on the right. Clusters with an asterisk after their names are likely to be old. Black lines are best-fitting King (1966) models; gray lines (most are directly over the black lines) are best-fitting Wilson (1975) models. Solid lines are model profiles after convolution with the PSF; dash-dotted lines are profiles before convolution. Note that the last four clusters are plotted with a different vertical scale.

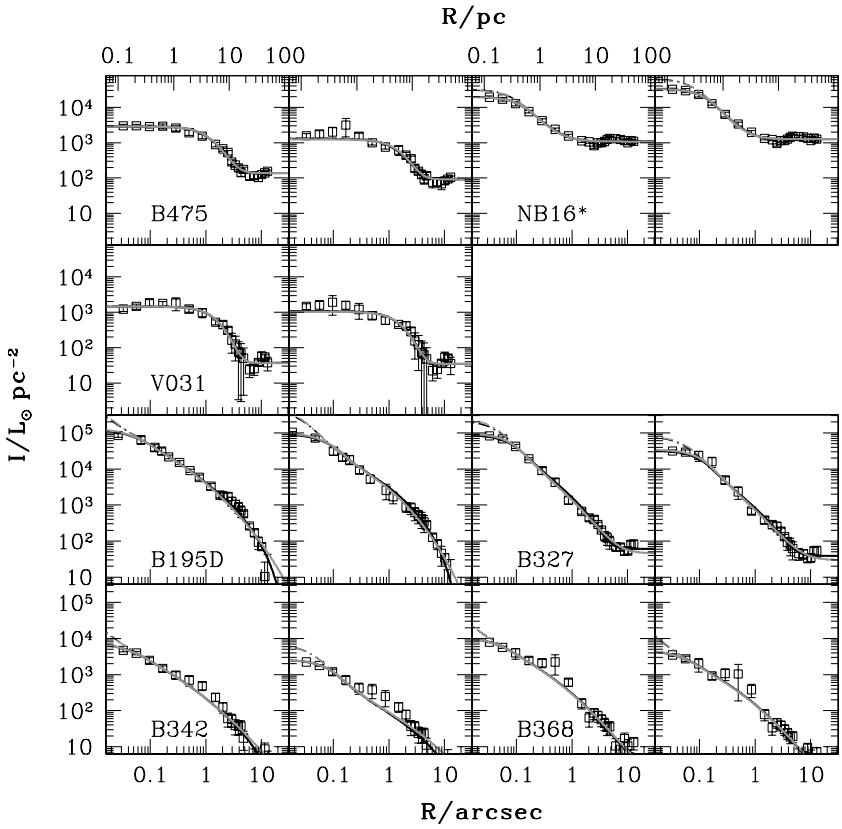

Figure 1. (Continued)

Table 3
Basic Parameters of Fits to Profiles of M31 Young Clusters

Name	Filter	N_{pts}	Model	χ^2_{min}	I_{bkg} ($L_\odot$ pc^{-2})	W_0	c	μ_0 (mag arcsec^{-2})	log r_0 (arcsec)	log r_0 (pc)
B015D	F450W	21	K66	323.12	7.5	$10.20^{+0.90}_{-0.80}$	$2.39^{+0.18}_{-0.17}$	$16.12^{+0.15}_{-0.15}$	$-0.640^{+0.108}_{-0.112}$	$-0.061^{+0.108}_{-0.112}$
			W	386.35	7.5	$10.80^{+1.10}_{-1.00}$	$3.38^{+0.13}_{-0.05}$	$16.11^{+0.16}_{-0.14}$	$-0.650^{+0.121}_{-0.111}$	$-0.071^{+0.121}_{-0.111}$
B015D	F814W	21	K66	231.70	12.8	$14.40^{+1.40}_{-1.00}$	$3.23^{+0.31}_{-0.21}$	$12.61^{+0.48}_{-0.69}$	$-1.758^{+0.196}_{-0.279}$	$-1.179^{+0.196}_{-0.279}$
			W	377.92	12.8	$14.90^{+1.50}_{-1.20}$	$4.15^{+0.39}_{-0.30}$	$12.47^{+0.51}_{-0.70}$	$-1.804^{+0.215}_{-0.287}$	$-1.225^{+0.215}_{-0.287}$
B040	F450W	21	K66	44.18	33.18 ± 3.56	$9.60^{+0.40}_{-0.30}$	$2.26^{+0.09}_{-0.07}$	$15.44^{+0.08}_{-0.11}$	$-0.967^{+0.048}_{-0.067}$	$-0.387^{+0.048}_{-0.067}$
			W	50.75	21.84 ± 5.10	$9.80^{+0.50}_{-0.40}$	$3.32^{+0.02}_{-0.00}$	$15.48^{+0.08}_{-0.10}$	$-0.931^{+0.054}_{-0.069}$	$-0.352^{+0.054}_{-0.069}$

Notes. Column descriptions—χ^2_{min}: unreduced χ^2 of best-fitting model; I_{bkg}: model-fit background intensity (values without uncertainties indicate clusters for which the background was fixed manually); W_0: model-fit central potential; $c = \log(r_t/r_0)$: model-fit concentration (r_t is tidal radius, given in Table 4); μ_0: model-fit central surface brightness; and log r_0: model-fit scale radius. Uncertainties are 68% confidence intervals, computed as described in the text.

(This table is available in its entirety in machine-readable and Virtual Observatory (VO) forms in the online journal. A portion is shown here for guidance regarding its form and content.)

the underlying cluster profile is actually a Wilson model. Using King models also allows us to compare the present sample to the combined sample of M31 globulars analyzed in Barmby et al. (2002, 2007): all of that sample has King fits while only about one-third has Wilson model fits. Because the focus of this paper is the young M31 clusters, dominated by blue stars, we use the F439W- or F450W-band measurements in preference to those from the redder filters.

The left panel of Figure 3 shows the properties of the present sample of clusters as a function of luminosity. Four clusters (vdB0, B327, B342, and B368) stand out as having very high central surface brightnesses; all except B327 also have correspondingly high concentrations. Figure 1 shows that the cores of these clusters do not appear to be resolved in our data. This could be due to the short exposure times: if the central cluster light is dominated by a few bright stars, the true integrated profile could be very difficult to recover. Structural parameters for these clusters are uncertain. Figure 1 also shows that the three M31 young clusters with the largest inferred half-light radii (B015D, B321, and B448) have relatively low contrast against the resolved stellar background of M31, so it is possible that the number counts include some field stars and the resulting R_h values are overestimates. The old cluster NB16 has a much smaller R_h and total luminosity than the other members of the sample: this cluster is projected on the M31 bulge, and its outer stars may be lost against the bright background. These issues highlight the limitations of our data set for the kind of structural analysis we are attempting, but the generally good match of model profiles with the observational ones gives us confidence that the cluster parameters we measure are reasonable.

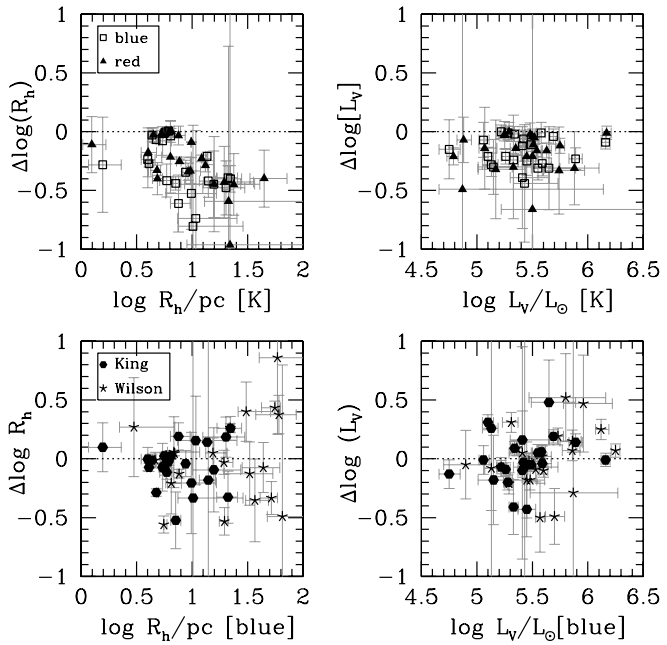

Figure 2. Comparison of half-light radii and total luminosity (converted to the *V* band) for Wilson and King models fit to surface brightness profiles of M31 young clusters. Bottom: comparison between observations of the same cluster in different filters (hexagons: King models, stars: Wilson models). Top: comparison of Wilson and King model fits to the same cluster (squares: red filter, triangles: blue filter).

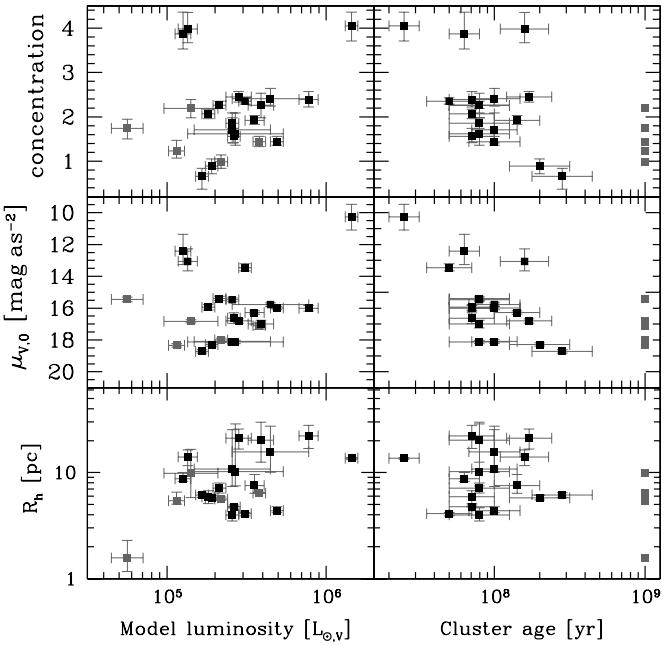

Figure 3. Concentration index, central surface brightness, and half-light radius for M31 young clusters as functions of total model luminosity (left) and estimated age (right). The old clusters are shown with gray symbols; although their ages are estimated at $>10^{10}$ yr, they are plotted at 10^9 yr in the right panel to condense the horizontal axis scale.

Analyzing the physical properties of M31 young clusters requires converting the observed flux-based measurements to luminosities and mass-linked quantities. Conversion from luminosity to mass is done using *V*-band mass-to-light ratios from the population synthesis models of Bruzual & Charlot (2003), assuming a Chabrier (2003) initial mass function (IMF) and solar metallicity for all but the oldest clusters. Table 1 lists the assumed ages for all clusters: those given by Perina et al. (2009b) for the young clusters from GO-10818, by Williams & Hodge (2001) for the clusters from GO-8296, and assumed ages of 13 Gyr for the clusters B083, B222, B347, B374 and NB16. We assume uncertainties of 10% in M/L_V and propagate these through the parameter estimates. While using M/L_V ratios determined directly from measured velocity dispersions would avoid the reliance on models, velocity dispersions are not available for most of the M31 clusters considered here. The use of a single set of population synthesis models also facilitates comparison of clusters in different galaxies; the comparison data for other galaxies (McLaughlin & van der Marel 2005; Barmby et al. 2007; McLaughlin et al. 2008) also used the same model mass-to-light ratios. Tables 4 and 5 give various derived parameters for the best-fitting models for each cluster (the details of their calculation are given by McLaughlin et al. 2008). Recently, Kruijssen & Lamers (2008) have discussed the time evolution of star cluster mass-to-light ratios due to preferential loss of low-mass stars with cluster age. This effect is expected to be most important for old clusters, and we have used the Kruijssen & Lamers models to confirm that the change in M/L for young clusters is minimal ($\lesssim$20%). Since our focus in this paper is the young M31 clusters, we therefore do not correct for this effect.

3. DISCUSSION: YOUNG AND OLD CLUSTERS IN M31 AND OTHER GALAXIES

Using star clusters as markers of the history of galaxies is aided by knowing how the clusters' structural properties change with age and environment. Although absolute ages of star clusters are notoriously difficult to determine, relative ages are more straightforward, and all of the clusters in our sample have ages estimated by CMD fitting (Williams & Hodge 2001; Perina et al. 2009b). Can we see evidence for changes in cluster properties with age? In the right panel of Figure 3, structural properties for the M31 young clusters are shown as a function of estimated age. None of the properties plotted depend on mass-to-light ratio, which is strongly dependent on age. Although our sample is small and covers a limited range in age, there is an interesting hint that central surface brightness becomes fainter and concentration decreases as age increases. This is consistent with the increase in core radius with age for MC clusters noted by Mackey & Gilmore (2003). Figure 4 explores this further by plotting μ_0, c, R_c, and central mass density ρ_0 for both the M31 young clusters and young clusters in the MCs. While the MC clusters also show a trend for central surface brightness to fade with age, it is much weaker than the trend implied by the M31 clusters alone, and the high surface brightness M31 clusters appear to be outliers (possibly artifacts due to the limited spatial resolution). Since the central mass density shows very little trend with age, the central surface brightness trend is likely due to fading of stellar population and the (weak) increase of core radius with age. The dashed line in the central surface brightness panel shows the effects of mass-to-light ratio change predicted by the Bruzual & Charlot (2003) models with a Chabrier (2003) IMF and solar metallicity; the slope shows a reasonable match to the cluster trend.

Figure 4 shows that, with a few exceptions, the young M31 clusters have similar spatial structure to young clusters in the MCs. A number of YMCs have recently been identified in the Milky Way; Pfalzner (2009) compiled size and mass measurements of these clusters (Figer 2008; Wolff et al. 2007) to argue that cluster evolution occurs along two well-defined tracks in

Table 4
Derived Structural and Photometric Parameters for M31 Young Clusters

Name	Filter	V Color (mag)	Model	log $r_{\rm tid}$ (pc)	log R_c (pc)	log R_h (pc)	log (R_h/R_c)	log I_0 ($L_{\odot,V}$ pc^{-2})	log j_0 ($L_{\odot,V}$ pc^{-3})	log L_V ($L_{\odot,V}$)	$V_{\rm tot}$ (mag)	log I_h ($L_{\odot,V}$ pc^{-2})	$\langle\mu_V\rangle_h$ (mag arcsec^{-2})
B015D	F450W	-0.114 ± 0.1	K66	$2.33^{+0.06}_{-0.07}$	$-0.065^{+0.106}_{-0.110}$	$1.346^{+0.100}_{-0.120}$	$1.411^{+0.210}_{-0.226}$	$4.16^{+0.07}_{-0.07}$	$3.92^{+0.17}_{-0.17}$	$5.89^{+0.06}_{-0.06}$	$14.59^{+0.15}_{-0.16}$	$2.39^{+0.20}_{-0.16}$	$20.42^{+0.39}_{-0.50}$
			W	$3.30^{+0.07}_{-0.00}$	$-0.076^{+0.118}_{-0.108}$	$1.746^{+0.061}_{-0.051}$	$1.821^{+0.170}_{-0.169}$	$4.16^{+0.07}_{-0.08}$	$3.93^{+0.17}_{-0.27}$	$6.12^{+0.07}_{-0.05}$	$13.99^{+0.14}_{-0.17}$	$1.83^{+0.08}_{-0.08}$	$21.82^{+0.20}_{-0.19}$
B015D	F814W	0.457 ± 0.1	K66	$2.05^{+0.03}_{-0.01}$	$-1.178^{+0.196}_{-0.279}$	$1.086^{+0.014}_{-0.001}$	$2.264^{+0.288}_{-0.194}$	$5.33^{+0.28}_{-0.20}$	$6.21^{+0.56}_{-0.39}$	$5.75^{+0.04}_{-0.04}$	$14.93^{+0.10}_{-0.11}$	$2.78^{+0.04}_{-0.04}$	$19.46^{+0.11}_{-0.10}$
			W	$2.93^{+0.10}_{-0.08}$	$-1.224^{+0.215}_{-0.286}$	$1.312^{+0.053}_{-0.025}$	$2.537^{+0.340}_{-0.240}$	$5.39^{+0.28}_{-0.21}$	$6.31^{+0.57}_{-0.42}$	$5.87^{+0.05}_{-0.05}$	$14.61^{+0.12}_{-0.13}$	$2.45^{+0.05}_{-0.09}$	$20.28^{+0.21}_{-0.12}$
B040	F450W	-0.029 ± 0.1	K66	$1.88^{+0.02}_{-0.02}$	$-0.393^{+0.047}_{-0.066}$	$0.853^{+0.047}_{-0.045}$	$1.245^{+0.113}_{-0.092}$	$4.40^{+0.06}_{-0.05}$	$4.49^{+0.12}_{-0.09}$	$5.33^{+0.04}_{-0.04}$	$15.98^{+0.10}_{-0.10}$	$2.82^{+0.09}_{-0.09}$	$19.34^{+0.23}_{-0.22}$
			W	$2.97^{+0.05}_{-0.05}$	$-0.361^{+0.052}_{-0.067}$	$1.292^{+0.022}_{-0.032}$	$1.652^{+0.089}_{-0.084}$	$4.39^{+0.06}_{-0.05}$	$4.54^{+0.04}_{-0.17}$	$5.57^{+0.04}_{-0.04}$	$15.37^{+0.11}_{-0.10}$	$2.19^{+0.06}_{-0.05}$	$20.93^{+0.13}_{-0.16}$

Notes. Column descriptions—r_t: model tidal radius ($\rho(r_t) = 0$); R_c: model projected core radius, at which intensity is half the central value; R_h: model projected half-light, or effective, radius (contains half the total luminosity in projection); R_h/R_c: measure of cluster concentration; I_0: model central luminosity surface density in the V band; j_0: logarithmic central luminosity volume density in the V band; L_V: total integrated model luminosity in the V band; $V_{\rm tot} = 4.83–2.5\,\log(L_V/L_\odot)+5\,\log(D/10\,{\rm pc})$: total, *extinction-corrected* apparent V-band magnitude; $I_h \equiv L_V/2\pi R_h^2$: V-band luminosity surface density averaged over the half-light radius; and $\langle\mu_V\rangle_h$: average surface brightness inside the half-light radius. Uncertainties are 68% confidence intervals, computed as described in the text.

(This table is available in its entirety in machine-readable and Virtual Observatory (VO) forms in the online journal. A portion is shown here for guidance regarding its form and content.)

Table 5
Derived Dynamical Parameters for M31 Young Clusters

Name	Filter	$\Upsilon_V^{\rm pop}$ ($M_\odot\,L_{\odot,V}^{-1}$)	Model	log $M_{\rm tot}$ ($M_\odot$)	log E_b (erg)	log Σ_0 ($M_\odot$ pc^{-2})	log ρ_0 ($M_\odot$ pc^{-3})	log Σ_h ($M_\odot$ pc^{-2})	log $\sigma_{\rm p,0}$ (km s^{-1})	log $v_{\rm esc,0}$ (km s^{-1})	log $t_{\rm rh}$ (yr)	log f_0 ($M_\odot$ (pc km s^{-1})$^{-3}$)
B015D	F450W	$0.088^{+0.01}_{-0.01}$	K66	$4.83^{+0.08}_{-0.08}$	$48.82^{+0.09}_{-0.09}$	$3.10^{+0.09}_{-0.09}$	$2.86^{+0.18}_{-0.18}$	$1.34^{+0.21}_{-0.16}$	$0.256^{+0.039}_{-0.042}$	$0.914^{+0.032}_{-0.034}$	$9.91^{+0.17}_{-0.20}$	$0.891^{+0.251}_{-0.242}$
			W	$5.07^{+0.08}_{-0.08}$	$48.91^{+4.13}_{-3.46}$	$3.11^{+0.08}_{-0.09}$	$2.88^{+0.18}_{-0.27}$	$0.78^{+0.09}_{-0.09}$	$0.251^{+0.076}_{-0.043}$	$0.924^{+0.548}_{-0.034}$	$10.61^{+0.12}_{-0.10}$	$0.915^{+0.250}_{-0.351}$
B015D	F814W	$0.088^{+0.01}_{-0.01}$	K66	$4.69^{+0.06}_{-0.07}$	$48.76^{+0.09}_{-0.09}$	$4.28^{+0.28}_{-0.20}$	$5.15^{+0.56}_{-0.39}$	$1.72^{+0.06}_{-0.07}$	$0.286^{+0.031}_{-0.033}$	$1.017^{+0.036}_{-0.036}$	$9.47^{+0.04}_{-0.03}$	$3.096^{+0.561}_{-0.395}$
			W	$4.82^{+0.07}_{-0.07}$	$48.80^{+0.09}_{-0.10}$	$4.33^{+0.29}_{-0.22}$	$5.25^{+0.57}_{-0.43}$	$1.40^{+0.07}_{-0.10}$	$0.290^{+0.031}_{-0.033}$	$1.028^{+0.035}_{-0.036}$	$9.87^{+0.10}_{-0.06}$	$3.184^{+0.578}_{-0.437}$
B040	F450W	$0.094^{+0.01}_{-0.01}$	K66	$4.30^{+0.06}_{-0.06}$	$48.25^{+0.09}_{-0.09}$	$3.38^{+0.07}_{-0.07}$	$3.46^{+0.12}_{-0.10}$	$1.80^{+0.10}_{-0.11}$	$0.229^{+0.031}_{-0.034}$	$0.875^{+0.030}_{-0.032}$	$8.94^{+0.08}_{-0.08}$	$1.570^{+0.148}_{-0.109}$
			W	$4.54^{+0.06}_{-0.06}$	$44.89^{+7.58}_{-0.09}$	$3.36^{+0.07}_{-0.07}$	$3.51^{+0.06}_{-0.18}$	$1.16^{+0.08}_{-0.07}$	$0.198^{+0.087}_{-0.032}$	$0.940^{+0.530}_{-0.062}$	$9.70^{+0.05}_{-0.06}$	$1.604^{+0.050}_{-0.183}$

Notes. Column descriptions—$\Upsilon_V^{\rm pop} L_V$: assumed mass-to-light ratio in the V band; $M_{\rm tot} = \Upsilon_V^{\rm pop} L_V$: integrated model mass; $E_b \equiv -(1/2)\int_0^{r_t} 4\pi r^2 \rho\phi\, dr$: integrated binding energy; Σ_0: central surface mass density; ρ_0: central volume density; Σ_h: surface mass density averaged over the half-light radius; $\sigma_{\rm p,0}$: predicted line-of-sight velocity dispersion at cluster center; $v_{\rm esc,0}$: predicted central "escape" velocity; log $t_{\rm rh}$: two-body relaxation time at model projected half-mass radius; and log $f_0 \equiv \log\left[\rho_0/(2\pi\sigma_c^2)^{3/2}\right]$: a measure of the model's central phase-space density or relaxation time. For f_0 in these units, and t_{rc} in years, $\log t_{rc} \simeq 8.28 - \log f_0$ (McLaughlin & van der Marel 2005). Uncertainties are 68% confidence intervals, computed as described in the text.

(This table is available in its entirety in machine-readable and Virtual Observatory (VO) forms in the online journal. A portion is shown here for guidance regarding its form and content.)

the density–radius plane. Using the conversion between Milky Way cluster size measurements and half-light radii described in the Appendix, we have compared cluster half-light radii and ages for the young Milky Way clusters together with the M31 and MC clusters in Figure 5. The M31 and MC clusters have similar sizes to the "leaky" Milky Way clusters but lie on the extrapolation of the age–R_h trend of the "starburst" MW clusters. This suggests that the starburst clusters (which tend to be more massive) are perhaps closer to being analogs of the YMCs in other galaxies. We speculate that the two evolutionary paths of Pfalzner (2009) may be simply due to extinction effects, with the "starburst" clusters having left their host cocoon and the "leaky" clusters still affected by excessive extinction in their outer regions (projection effects may also be important). This would imply that starburst clusters are more easily identified in external galaxies, explaining the reasonable match between extragalactic young clusters and Milky Way starburst clusters.

An important question in the study of YMCs is whether they will eventually become old massive clusters resembling the GCs we see today in the Galaxy. Once formed, star clusters have no easy way to gain mass, but they do have a number of ways to lose mass or even be completely disrupted (Spitzer 1987; Vesperini 1998; Lamers & Gieles 2006). We have computed dissolution times for our cluster sample considering the effects of both the stellar and dynamical evolution of star clusters through time. These calculations explicitly account for age, metallicity, and half-light radius of all sample star clusters, and treat the effects of evaporation of low-mass stars, mass loss due to stellar evolution, encounters with spiral arms and giant molecular clouds following in part the prescriptions of Lamers et al. (2005) and Lamers & Gieles (2006). The results are shown in Figure 6. All clusters have dissolution time greater than their ages; however, for two young clusters (B321 and B342) and the old cluster B374, these quantities are nearly equal, suggesting that they are in the process of dissolving. On average, the young clusters' dissolution times are too short to expect them to become old ($>10^{10}$ yr) clusters. However, a few have $t_d > 1$ Gyr and, if they avoid collisions with giant molecular clouds, might survive to become sparse old globulars. In general, the dissolution times confirm the importance of cluster dissolution to the evolution of the star cluster mass function (see also, e.g., Gnedin & Ostriker 1997; Gieles 2009). Lower-mass and/or more-diffuse clusters in M31, such as those discovered by Krienke & Hodge (2007, 2008) and Hodge et al. (2009), would be even more likely to dissolve.

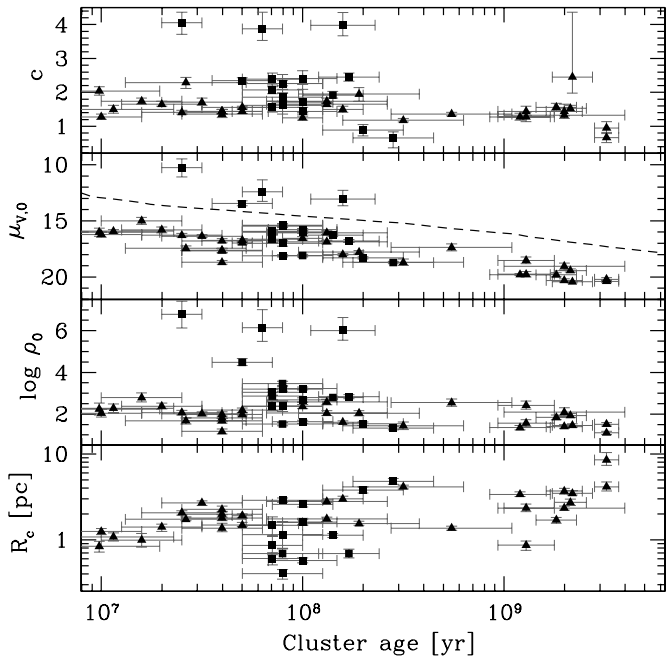

Figure 4. Concentration index, central surface brightness, and central mass density for M31 (squares) and Magellanic Cloud (triangles) young clusters as functions of estimated age. The dashed line in the central surface brightness panel shows the expected change in surface brightness due to changes in mass-to-light ratio with age (vertical normalization is arbitrary).

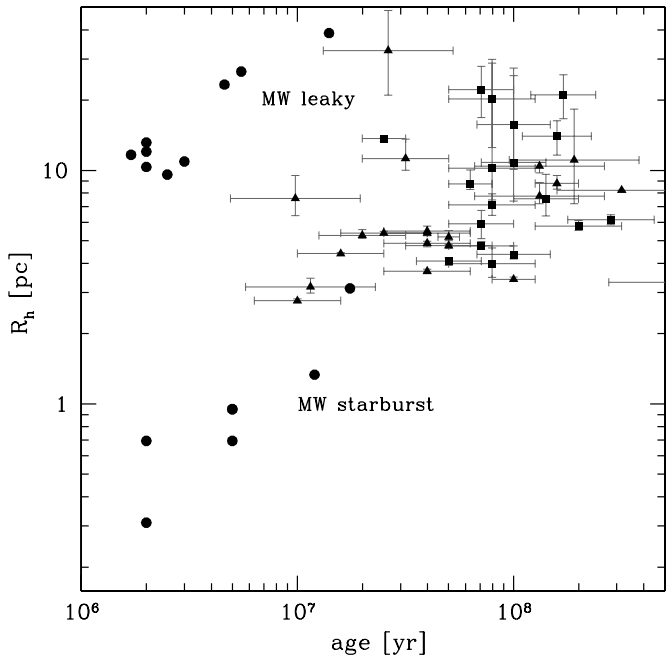

Figure 5. Young star cluster ages and sizes. Squares: M31 clusters from the present sample; triangles: young Magellanic Cloud clusters; and circles: young massive Milky Way clusters from Figer (2008) and Wolff et al. (2007). The two groups of Milky Way clusters identified by Pfalzner (2009) are labeled.

Work to date suggests that the structural parameters of old star clusters in several nearby galaxies show only a weak dependence on environment (Barmby et al. 2007), and the comparisons above indicate that young clusters in different galaxies are also similar. How do young and old clusters compare? Figure 7 shows cluster properties as a function of mass for M31 young clusters, MC young clusters and Milky Way globulars (McLaughlin & van der Marel 2005), M31 globulars (Barmby et al. 2002, 2007),

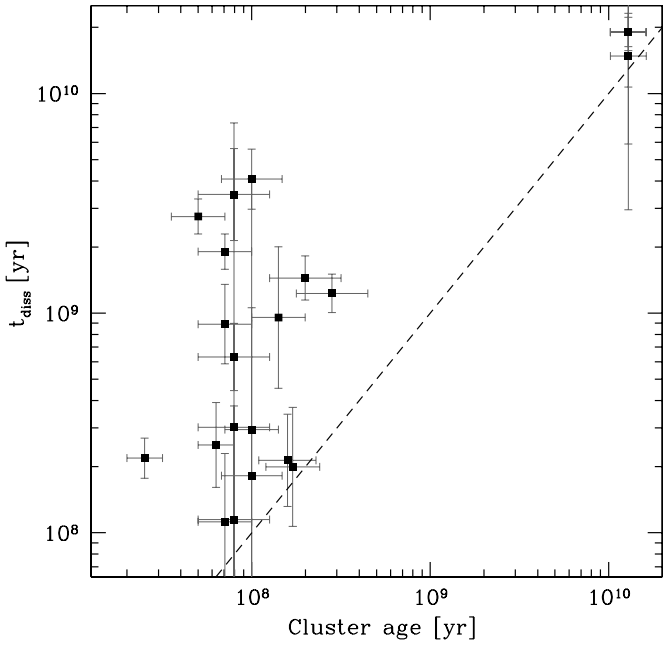

Figure 6. Dissolution times for M31 star clusters, compared to cluster ages. Four of the five old clusters are plotted at the same position, with dissolution times 20 Gyr and assumed ages 13 Gyr.

and recently discovered extended M31 halo clusters (Huxor et al. 2005).[12] The joint mass–age distribution of the clusters differs by galaxy: some of this is due to complex selection effects (e.g., the M31 globular sample is incomplete and biased toward more luminous clusters, and the sample of Milky Way YMCs is also incomplete), but there are hints of real differences between galaxies; see Perina et al. (2009b) for a more detailed discussion. The properties of the five old clusters in our sample are similar to those of M31 and Milky Way globulars, while the properties of M31 young clusters overlap with those of both the young MC clusters and the low-mass Milky Way GCs. Thus, the M31 young clusters do not appear to be fundamentally different types of object from those already known. On average, the younger clusters have larger sizes and higher concentrations (where larger c implies a larger tidal radius for the same scale radius) than old clusters of the same mass. The young clusters therefore have larger tidal radii, which makes them more susceptible to dynamical destruction: small-r_t clusters are more likely to survive to old age. The larger spread in properties of low-mass clusters compared to higher-mass clusters may indicate lower data quality for these fainter objects, rather than an intrinsic difference in properties.

By now it is well known that old star clusters in the Milky Way and other galaxies describe an FP in structural properties (Djorgovski 1995; Djorgovski et al. 1997), although the separation of clusters from other types of objects has become less well defined in recent years. The results of Bastian et al. (2006) and Kissler-Patig et al. (2006) indicate that YMCs fall on FPs similar to those of old clusters. Those results make use of cluster velocity dispersions, while in this work, we must use mass-to-light ratios from population synthesis models applied

[12] Mass measurements for all clusters are derived using mass-to-light ratios. As discussed in Section 2.4, these ratios are affected by cluster dynamical evolution. Correcting for this effect is non-trivial and beyond the scope of this paper; however, the results of Kruijssen (2008) imply that doing so would increase the spread of the old clusters' mass distribution and shift it to lower masses.

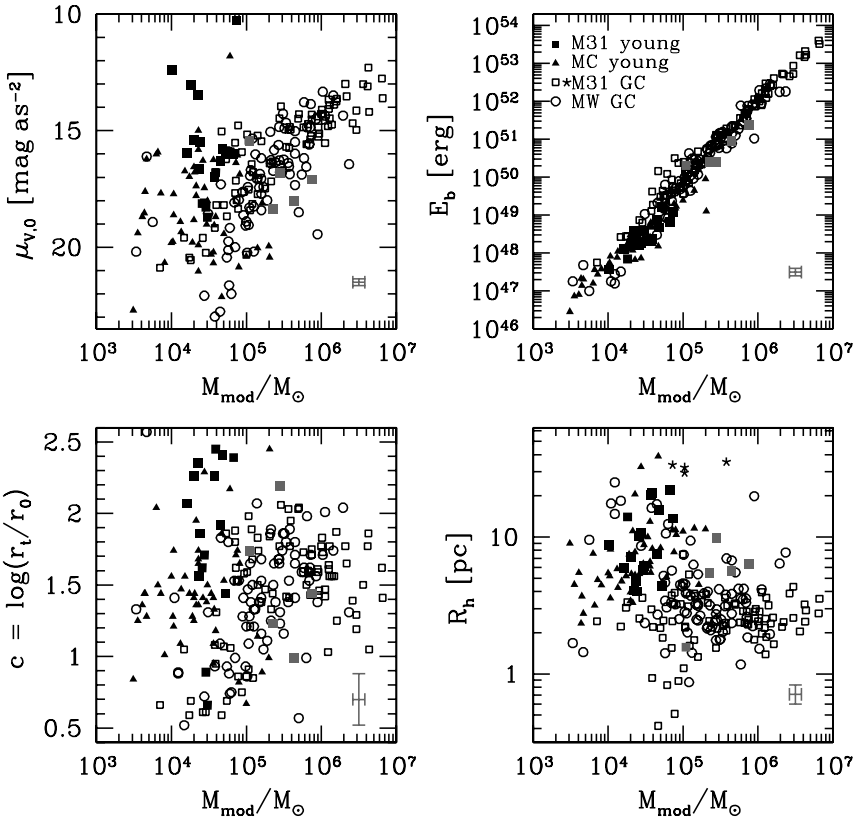

Figure 7. Structural properties of young and old star clusters in M31, young clusters in the Magellanic Clouds, and globular clusters in the Milky Way, shown as a function of cluster mass. Top left: central surface brightness; top right: binding energy; lower left: concentration; and lower right: half-light radius. Filled squares: M31 clusters from the present sample (black: young clusters, gray: old clusters); open squares: old M31 clusters from Barmby et al. (2007, 2002); stars: "extended luminous clusters" in M31 from Huxor et al. (2005); and filled triangles: young Magellanic Cloud clusters. Error bars show median uncertainties for the young M31 clusters.

to the photometry instead of independent mass estimates. The upper-right panel of Figure 7 shows one view of the FP, as defined by McLaughlin (2000). The old clusters in our sample fall nicely on this relation, as do most of the younger clusters. The observed correlation between mass and binding energy E_b is expected, since by definition $E_b = f(c)M^2/R_h$, where $f(c)$ is a weak function of cluster concentration c. However, the tightness of the correlation shows that there is very little relation between young cluster mass and R_h (see also lower right panel), and no offsets in the basic properties of the cluster shapes between old and young clusters.

Figure 8 shows a different view of the FP, more akin to the parameters usually shown for elliptical galaxies (see also McLaughlin 2003; Strader et al. 2009). The left two panels show the surface-brightness-based FP relations, with a large offset between the young M31 and MC clusters (light gray symbols) and the old clusters. This is to be expected because of the young clusters' lower mass-to-light ratios. When we instead plot quantities related to the mass density (right panels), the young clusters fall on the same relations as the old clusters. The tightness of the relations primarily reflects the use of mass-to-light ratios to compute both central velocity dispersion σ_0 and mass density Σ. Again, however, the lack of offset and similar scatter between the young and old clusters confirms their similar overall structures. Recent measurements of M31 GCs' mass-to-light ratios (Strader et al. 2009) have shown that these clusters do follow the FP relations as expected from model mass-to-light ratios. Similar measurements for young clusters should show whether young clusters do the same. If so, this would indicate that the FP reflects conditions of cluster formation and is not merely the end product of cluster dynamical evolution.

Bonatto & Bica (2005) argue that Milky Way OCs fall on a plane in the three-dimensional space of total mass, core radius, and projected core mass density. We can compare this space to the FP using an approximate relation between mass and central velocity dispersion. The least-squares fit for the young MC clusters (the most populous sample of young clusters available) gives $\log \sigma_0 = 0.34 \log M - 1.38$; combined with the Bonatto & Bica (2005) cluster parameters, we find that the Milky Way OCs fall approximately on the other young clusters with $\Sigma_0 \sim 10^2\ M_\odot\ \mathrm{pc}^{-2}$ in the top right panel of Figure 8. This suggests that the Milky Way OC plane indicated by Bonatto & Bica (2005) may in fact be the same FP defined by other star clusters, which have projected mass densities higher by up to 4 orders of magnitude. As Bonatto & Bica (2005) discuss, this result remains to be confirmed with large samples, but it is certainly intriguing in its implications for a "universal" star cluster FP.

4. SUMMARY AND DIRECTIONS FOR FUTURE WORK

This series of papers has established that a sample of candidate young star clusters in M31 is indeed young, massive clusters, with properties similar to those of other young clusters in Local Group galaxies. Our current data do not allow us to detect the extended haloes characterized by Wilson models and seen in other young clusters; the more compact King models provide adequate fits to the data. The structural parameters

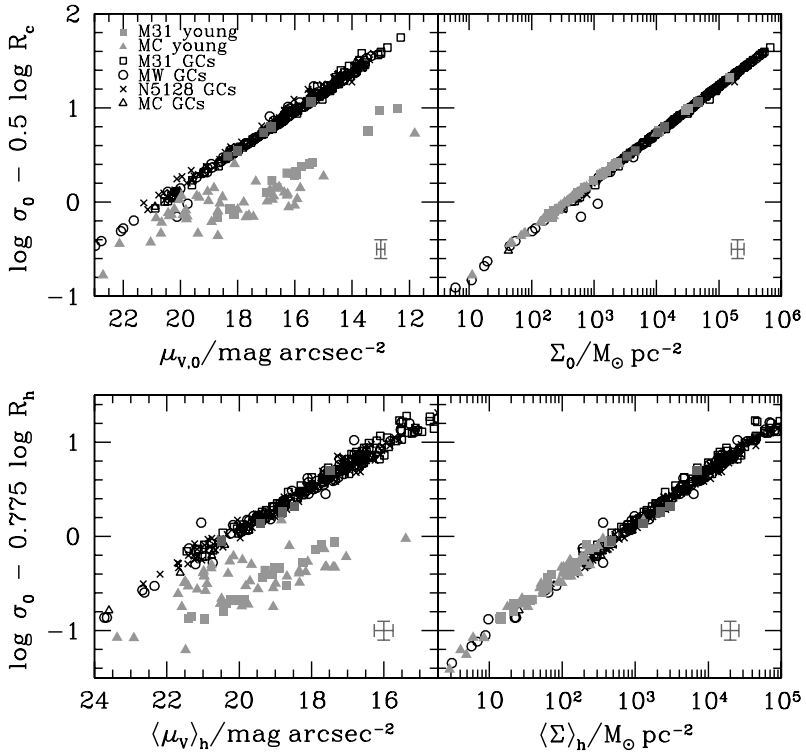

Figure 8. Views of the star cluster fundamental plane, with core parameter relations in the bottom panels and half-light parameter relations in the top panels. σ_0 is predicted central velocity dispersion and Σ represents surface mass density either in the cluster core or at the half-light radius. Left panels show surface brightness while right panels show mass surface density. Filled squares: M31 clusters from the present sample (light gray: young clusters, dark gray: old clusters); open triangles: old Magellanic Cloud and Fornax clusters; open circles: Milky Way globulars; and crosses: NGC 5128 globulars. Other symbols as in Figure 7. Error bars show median uncertainties for the young M31 clusters.

measured in this paper show the M31 clusters to be typical young clusters, with masses of 10^4–$10^5\ M_\odot$, half-light radii of 3–20 pc, and dissolution times of <5 Gyr. While the basic similarity between young clusters in different Local Group galaxies, and between young and old clusters, seems well established, many questions remain. What is the precise form of the age–size relation? Do cluster mass-to-light ratios evolve with age as predicted by dynamical and stellar evolution models? What fraction of the stellar disk in galaxies is comprised of dissolving clusters? Is there a relation between the cluster formation and local star formation rate, or other galaxy properties? Large cluster samples with high-quality data will be needed to address these and other questions about the relationship and history of star clusters and their parent galaxies.

Facilities: HST (WFPC2)

We thank D.E. McLaughlin for the use of the GRIDFIT software. P.B. acknowledges research support through a Discovery Grant from the Natural Sciences and Engineering Research Council of Canada and an Ontario Early Researcher Award. S.P. and M.B. acknowledge the financial support of INAF through PRIN 2007 grant No. CRA 1.06.10.04: "The local route to galaxy formation." J.G.C. acknowledges support from NASA from grant GO-10818. T.H.P acknowledges support through the Plaskett Research Fellowship at the Herzberg Institute of Astrophysics.

APPENDIX

ARTIFICIAL CLUSTER TESTS

Deriving surface brightness profiles of star clusters in Local Group galaxies requires careful analysis. The clusters are only partially resolved into individual stars, and they are observed together with a galactic background which may also be resolved into stars. The purpose of this section is to investigate the best methods for extracting structural parameters of "semi-resolved" clusters, particularly from relatively shallow images, and to quantify the uncertainties of those parameters. This can best be done by analyzing profiles derived from images of artificial clusters whose structural parameters are known. A related study by Noyola & Gebhardt (2006) simulated integrated photometry from *HST* observations of Galactic GCs; however, the focus of that study was on recovering the structure of cluster cores rather than overall structure. Bonatto & Bica (2008) also carried out a similar study, but considering only King (1962) models for Galactic clusters.

The first step in analyzing simulated star cluster profiles is to determine the type of model profile and range of parameter space to be covered. The analysis of McLaughlin & van der Marel (2005) showed that Wilson models were adequate to describe both Milky Way and MC cluster profiles, so we chose this set of models for our artificial clusters. Since we are interested in differences between young and old clusters, we examined the distribution of scale radius r_0 and central potential W_0 for both young and old MC clusters as given by McLaughlin & van der Marel (2005): W_0 ranged from 1 to 10 with a typical value $W_0 \approx 5$, while r_0 ranged from 0.2 to 20 pc with a typical value $r_0 \approx 2$ pc. The range of implied half-light radii is 1–35 pc.

Our artificial clusters were generated from Wilson profiles with eight values of r_0 between 0.5 and 11 pc, and nine values of W_0 between 2 and 10. For each (W_0, r_0) pair, we generated clusters with four different population sizes: $N_* =$ 100, 300, 1000, and 3000. The stars' projected spatial positions were generated by selecting the projected radial coordinate from

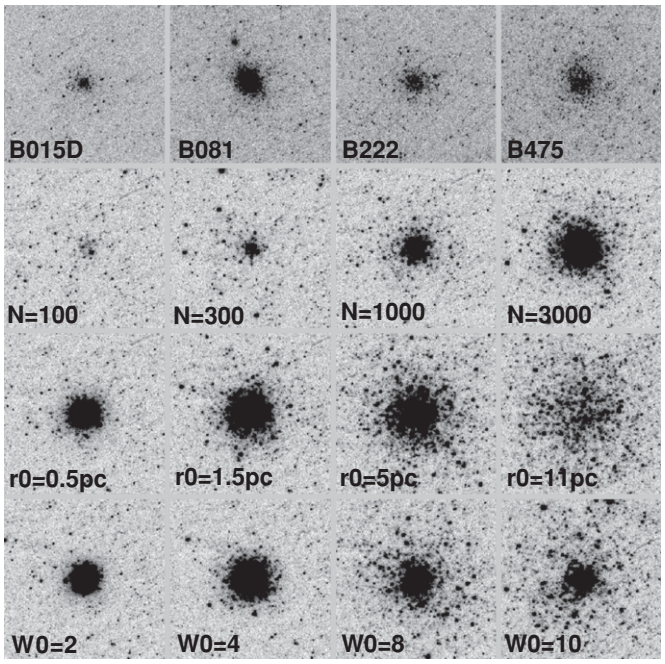

Figure 9. Top row: four M31 star clusters observed as part of program GO-10818 with the *HST*. Left to right: B015D, B081, B222, and B475. Second row: simulated clusters with central potential $W_0 = 6$ and scale radius $r_0 = 2$ pc, with (left to right) $N_* = 100$, 300, 1000, and 3000. Third row: simulated clusters with $N_* = 3000$, central potential $W_0 = 6$, and scale radius (left to right) $r_0 = 0.5$, 1.5, 5, and 11 pc. Fourth row: simulated clusters with $N_* = 3000$, scale radius $r_0 = 2$ pc, and (left to right) $W_0 = 2$, 4, 8, and 10. All images are 800 s exposures in the F450W filter on the WFPC2/PC chip; each subimage is 13.7 × 13.7 arcsec (51.7 × 51.7 pc at the distance of M31).

the probability distribution associated with the Wilson profile,

$$p(R) = \frac{R\,\Sigma_{W_0,r_0}(R)}{\int_0^{R_{\max}} \Sigma(R')R'\,dR'}, \qquad \text{(A1)}$$

and generating the angular coordinate θ at random. The stars' luminosities were generated by selecting from an observed "young cluster" luminosity distribution, uncorrected for completeness. The distribution was generated by combining the observed magnitudes of stars in the four most populous clusters in the GO-10818 program (VdB0, B257D, B475, and B327). Separate luminosity distributions were used in each of the two observational bands.

The specific observations being modeled are the same as those in the GO-10818 program. We generated images of the simulated clusters by inserting artificial stars modeled with the appropriate PSF near the center of a WFPC2/PC image of a field in M31. The background images used were the observations of "B195D" from the GO-10818 program; the PC chip was essentially empty in this observation because of an error in the input coordinates (for details, see Perina et al. 2009a). This field is located in the southwest disk of M31. Figure 9 shows a sample of the simulated cluster images, together with some sample M31 clusters for comparison. The simulated clusters cover a wider range of properties than the real clusters: some of the simulated clusters were in fact not visually apparent in the images. These "clusters" had few stars ($N_* = 100$ or $N_* = 300$) and very large half-light radii, more akin to dwarf galaxies than to objects recognizable as star clusters. They are not considered further in this analysis.

Surface density profiles for the simulated clusters were derived in several different ways. The first method ("number counts") derived the surface density as simply the number of stars per unit area in annular bins. Since the locations of all stars are known precisely for the simulated clusters, this method represents the best possible data for surface density profiles. Deriving structural parameters from such data tests the fitting routine itself and also the extent to which density profiles can be derived from a limited number of stars. Stars were counted in overlapping annular bins of width 3 pixels (0.5 pc) inside a radius of 20 pixels (3.4 pc) and width 10 pixels (1.7 pc) outside this radius.

For real star clusters, crowding limits the ability to resolve individual stars and hence derive surface density profiles through number counts. We also derived surface density profiles of clusters using isophotal photometry with the IRAF ELLIPSE package, similar to the method described in Barmby et al. (2007). We refer to this as the "integrated photometry" method. We also combined the number count and integrated photometry methods in a "hybrid" method similar to that used by Federici et al. (2007). This involves matching the intensity scales of the two profiles by fitting both profiles to smooth curves in the region $r = 5$–10 pc. The switch-over from integrated photometry to number counts was made at a radius of 7 pc (40.6 pixels), where in general both types of profile had good signal to noise.

Wilson models were fitted to the artificial cluster data using the GRIDFIT program described in Section 2.3. As for the real clusters, instrumental PSF profiles were convolved with the model profiles before comparison to the data. Unlike the real clusters, however, the background level for the artificial clusters was fixed at zero. For clusters of all sizes, the number count input returned fitted parameters in good agreement with the input parameters. The offsets between input and output parameters are (mean ± standard error) $\Delta W_0 = (W_{0,\rm in} - W_{0,\rm out})/W_{0,\rm in} = 0.06 \pm 0.02$ and $\Delta r_0 = (r_{0,\rm in} - r_{0,\rm out})/r_{0,\rm in} = -0.13 \pm 0.03$ pc. As expected, the larger-N_* clusters return more accurate values, with scatter 2–3 times lower for $N_* = 3000$ than for $N_* = 300$ clusters. Figure 10 compares the best-fit and input structural parameters of the simulated clusters for the integrated photometry and hybrid methods. Particularly for clusters with larger input r_0, integrated photometry alone tends to result in overly large values of W_0 and overly small values of r_0. For these clusters, the distinction between profiles of different W_0's occurs at a point in the radial profile where the density of stars is too low for the ELLIPSE algorithm to converge. The addition of number count data beyond this point improves the fit, as the figure shows. For integrated photometry alone, $\Delta W_0 = -0.56 \pm 0.07$ and $\Delta r_0 = 0.24 \pm 0.04$ pc; for the hybrid method, $\Delta W_0 = -0.02 \pm 0.02$ and $\Delta r_0 = -0.05 \pm 0.03$ pc.

When fitting model profiles to cluster data, the correct model family is not known a priori. What happens if artificial "Wilson" clusters are fitted with King models instead? We tried this experiment with our artificial clusters and were surprised to find that, except for a handful of objects, the two model families returned nearly identical χ^2 values: the median fractional difference $(\chi^2_{\rm K} - \chi^2_{\rm W})/\chi^2_{\rm W} = 0.01$. While the meaning of model parameters such as the scale radius r_0 differs between model families, some derived quantities such as the core and half-light radii (R_c, R_h; see Table 4 for description) are directly comparable. Figure 11 shows this comparison. There is very good agreement between the two model families in measurements of core radii, and reasonable agreement in measurements of half-light radii. The agreement in R_h is poorer for the largest clusters ($R_h \gtrsim 20$ pc, a larger size than usually seen in real clusters), where the King models return smaller sizes than the Wilson

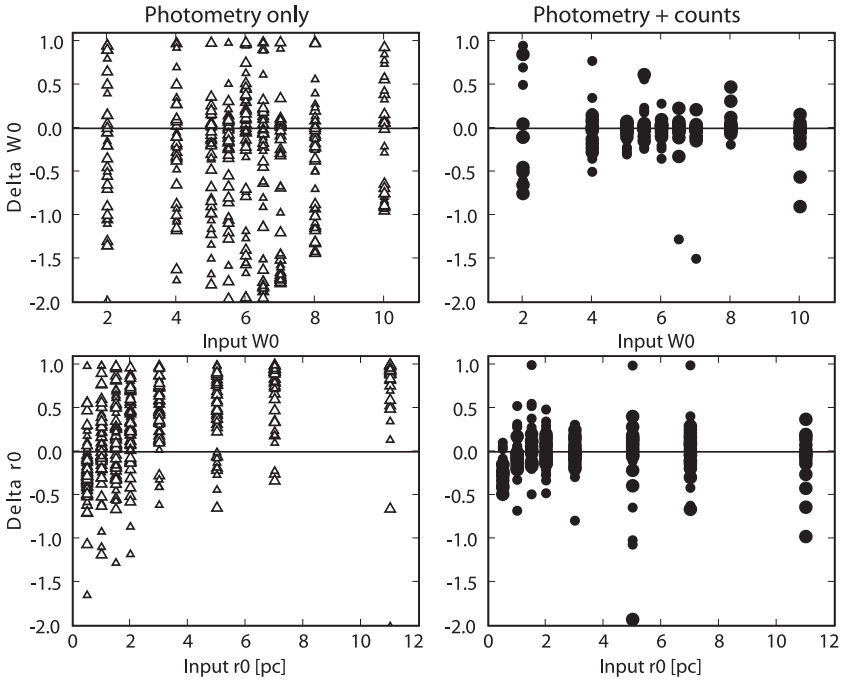

Figure 10. Comparison of input and output structural parameters for simulated star clusters. The output parameters are derived from fitting Wilson models to surface density profiles derived from simulated *HST*/WFPC2 images of the clusters. Left: profiles measured with integrated photometry only; right: profiles measured with integrated photometry and number counts; top: difference in central potential $\Delta W_0 = (W_{0,\rm in} - W_{0,\rm out})/W_{0,\rm in}$; and bottom: difference in scale radius $\Delta r_0 = (r_{0,\rm in} - r_{0,\rm out})/r_{0,\rm in}$.

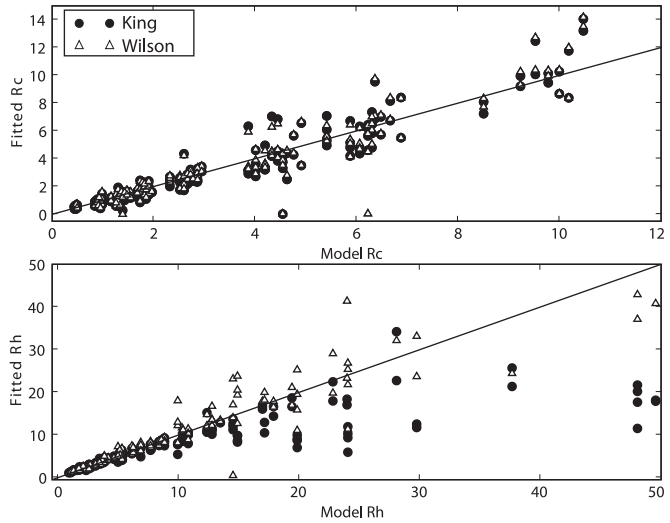

Figure 11. Comparison of cluster size measurements for fits of model density profiles to artificial cluster profiles. Top: core radius R_c; bottom: half-light radius R_h; circles: King (1966) model fits; and triangles: Wilson (1975) model fits.

models. This is consistent with the results of McLaughlin & van der Marel (2005) who found that the two model families gave generally consistent results for Milky Way and MC clusters as long as the radius of the last data point $R_{\rm last} \gtrsim 5R_h$.

The situation of observational profiles with a limited radial range bears further investigation. The analysis of simulated clusters to this point has not considered the effects of background level fluctuations. The GRIDFIT code is able to fit a constant background level added to the intensity profile, and we verified through simple experiments that input values were correctly recovered. However, the limitations of short exposures and small-number statistics suggest that determining the correct background level—and thus being able to correctly trace cluster profiles out to large projected radii—will be much more difficult for the real cluster data. We therefore experimented with removing points in the profile data beyond $R_{\rm last} = 1$, 2, and $5R_h$ (where R_h was computed from the input model profile) and fitting both King and Wilson models to the remaining points. As expected, recovery of the input cluster parameters was better for the more extensive profiles, for both model families. For $R_{\rm last} = 1$, both model families returned R_h values that were, on average, larger than the input. Some model fits were "catastrophic failures," with $R_h(\rm out) > 2R_h(\rm in)$; this situation usually occurred for clusters where the number of profile data points was <10. Interestingly, for all three values of $R_{\rm last}$, King model fits had fewer catastrophic failures than Wilson models, and also slightly smaller scatter in the difference between fit and true parameters. Since the primary difference between King and Wilson model profiles is the more extended halo of the latter, this suggests that King models may be a better choice for fitting noisy cluster profiles.

Finally, we considered the issue of comparison between different measurements of star cluster size. While Milky Way globulars and extragalactic clusters are most often characterized with half-light or core radii, recent compilations of data for massive young Milky Way clusters (Figer 2008; Wolff et al. 2007) measure cluster size as the mean or median distance ($\langle R \rangle$ or $\tilde{R}$) of the cluster stars from the geometric centroid. Since these young Milky Way clusters may well not be dynamically relaxed (Goodwin & Bastian 2006), it may not make sense to fit the same types of dynamical models to them as to old clusters, but it is still desirable to find a way to compare sizes between groups of clusters. Since we know the positions of all stars in our artificial clusters, we can easily compute the statistical measurements of size for our model clusters, and

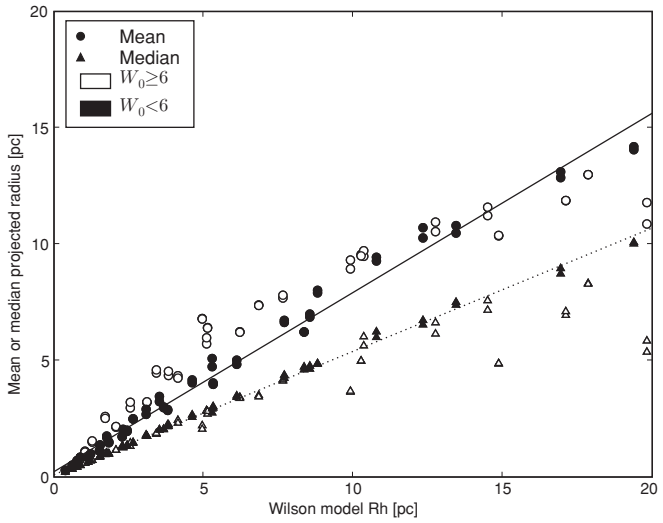

Figure 12. Comparison of model half-light radius R_h to mean and median projected radius for artificial clusters. Circles: mean; triangles: median; filled symbols: models with $W_0 < 6$; and open symbols: models with $W_0 \geqslant 6$. Solid line: least-squares fit to filled circles; dotted line: least-squares fit to filled triangles.

compare them to (model values of) R_c and R_h. $\langle R \rangle$ and $\tilde{R}$ are very well correlated for all of our model clusters, with a best-fit linear relation $\tilde{R} = 0.67\langle R \rangle - 0.36$. The correlation between $\langle R \rangle$ and R_c is rather poor (unsurprising as R_c depends critically on the exact shape of the cluster profile), but there is a good match between $\langle R \rangle$ and R_h for models that are not too extended ($W_0 \lesssim 6$). Figure 12 shows the data and least-squares fits: $\langle R \rangle = 0.77R_h + 0.23$, and $\tilde{R} = 0.53R_h + 0.10$. We conclude that, with some scaling, the mean or median projected separation of stars from a cluster center are reasonable proxies for the half-light radius.

REFERENCES

Barmby, P., Holland, S., & Huchra, J. P. 2002, AJ, 123, 1937
Barmby, P., Huchra, J. P., Brodie, J. P., Forbes, D. A., Schroder, L. L., & Grillmair, C. J. 2000, AJ, 119, 727
Barmby, P., McLaughlin, D. E., Harris, W. E., Harris, G. L. H., & Forbes, D. A. 2007, AJ, 133, 2764
Bastian, N., Saglia, R. P., Goudfrooij, P., Kissler-Patig, M., Maraston, C., Schweizer, F., & Zoccali, M. 2006, A&A, 448, 881
Bendinelli, O., et al. 1993, ApJ, 409, L17
Bica, E., Bonatto, C., Dutra, C. M., & Santos, J. F. C. 2008, MNRAS, 389, 678
Bonatto, C., & Bica, E. 2005, A&A, 437, 483
Bonatto, C., & Bica, E. 2008, A&A, 477, 829
Brodie, J. P., Schroder, L. L., Huchra, J. P., Phillips, A. C., Kissler-Patig, M., & Forbes, D. A. 1998, AJ, 116, 691
Bruzual, G., & Charlot, S. 2003, MNRAS, 344, 1000
Caldwell, N., Harding, P., Morrison, H., Rose, J. A., Schiavon, R., & Kriessler, J. 2009, AJ, 137, 94
Chabrier, G. 2003, PASP, 115, 763
Cohen, J. G., & Freeman, K. C. 1991, AJ, 101, 483
Cohen, J. G., Matthews, K., & Cameron, P. B. 2005, ApJ, 634, L45
Djorgovski, S. 1995, ApJ, 438, L29
Djorgovski, S., & King, I. R. 1986, ApJ, 305, L61
Djorgovski, S., & Meylan, G. 1994, AJ, 108, 1292
Djorgovski, S. G., Gal, R. R., McCarthy, J. K., Cohen, J. G., de Carvalho, R. R., Meylan, G., Bendinelli, O., & Parmeggiani, G. 1997, ApJ, 474, L19
Elson, R. A. W., Fall, S. M., & Freeman, K. C. 1987, ApJ, 323, 54
Federici, L., Bellazzini, M., Galleti, S., Fusi Pecci, F., Buzzoni, A., & Parmeggiani, G. 2007, A&A, 473, 429
Figer, D. F. 2008, in IAU Symp. 250, Massive Stars as Cosmic Engines, ed. F. Bresolin, P. A. Crowther, & J. Puls (Dordrecht: Kluwer), 247
Fusi Pecci, F., Bellazzini, M., Buzzoni, A., De Simone, E., Federici, L., & Galleti, S. 2005, AJ, 130, 554
Fusi Pecci, F., et al. 1994, A&A, 284, 349
Galleti, S., Bellazzini, M., Federici, L., Buzzoni, A., & Fusi Pecci, F. 2007, A&A, 471, 127
Galleti, S., Federici, L., Bellazzini, M., Fusi Pecci, F., & Macrina, S. 2004, A&A, 416, 917
Gieles, M. 2009, MNRAS, 394, 2113
Gnedin, O. Y., & Ostriker, J. P. 1997, ApJ, 474, 223
Goodwin, S. P., & Bastian, N. 2006, MNRAS, 373, 752
Grillmair, C. J., Ajhar, E. A., Faber, S. M., Baum, W. A., Holtzman, J. A., Lauer, T. R., Lynds, C. R., & O'Neil, E. J., Jr. 1996, AJ, 111, 2293
Haşegan, M., et al. 2005, ApJ, 627, 203
Hodge, P. W., Krienke, O. K., Bellazzini, M., Perina, S., Barmby, P., Cohen, J. G., Puzia, T. H., & Strader, J. 2009, AJ, 138, 770
Holland, S., Fahlman, G. G., & Richer, H. B. 1997, AJ, 114, 1488
Holtzman, J. A., et al. 1992, AJ, 103, 691
Hubble, E. 1932, ApJ, 76, 44
Huxor, A. P., Tanvir, N. R., Irwin, M. J., Ibata, R., Collett, J. L., Ferguson, A. M. N., Bridges, T., & Lewis, G. F. 2005, MNRAS, 360, 1007
Jordán, A. 2004, ApJ, 613, L117
Kharchenko, N. V., Piskunov, A. E., Röser, S., Schilbach, E., & Scholz, R.-D. 2005, A&A, 438, 1163
King, I. 1962, AJ, 67, 471
King, I. R. 1966, AJ, 71, 64
Kissler-Patig, M., Jordán, A., & Bastian, N. 2006, A&A, 448, 1031
Krienke, O. K., & Hodge, P. W. 2007, PASP, 119, 7
Krienke, O. K., & Hodge, P. W. 2008, PASP, 120, 1
Kruijssen, J. M. D. 2008, A&A, 486, L21
Kruijssen, J. M. D., & Lamers, H. J. G. L. M. 2008, A&A, 490, 151
Lamers, H. J. G. L. M., & Gieles, M. 2006, A&A, 455, L17
Lamers, H. J. G. L. M., Gieles, M., Bastian, N., Baumgardt, H., Kharchenko, N. V., & Portegies Zwart, S. 2005, A&A, 441, 117
Larsen, S. S. 2004, A&A, 416, 537
Larsen, S. S., & Richtler, T. 1999, A&A, 345, 59
Mackey, A. D., & Gilmore, G. F. 2003, MNRAS, 338, 85
McLaughlin, D. E. 2000, ApJ, 539, 618
McLaughlin, D. E. 2003, in ASP Conf. Ser. 296, New Horizons in Globular Cluster Astronomy, ed. G. Piotto et al. (San Francisco, CA: ASP), 101
McLaughlin, D. E., Barmby, P., Harris, W. E., Forbes, D. A., & Harris, G. L. H. 2008, MNRAS, 384, 563
McLaughlin, D. E., & van der Marel, R. P. 2005, ApJS, 161, 304
Meylan, G., & Djorgovski, S. 1987, ApJ, 322, L91
Noyola, E., & Gebhardt, K. 2006, AJ, 132, 447
Perina, S., et al. 2009a, A&A, 494, 933
Perina, S., et al. 2009b, A&A, submitted
Pfalzner, S. 2009, A&A, 498, L37
Piskunov, A. E., Schilbach, E., Kharchenko, N. V., Röser, S., & Scholz, R.-D. 2007, A&A, 468, 151
Piskunov, A. E., Schilbach, E., Kharchenko, N. V., Röser, S., & Scholz, R.-D. 2008, A&A, 477, 165
Racine, R. 1991, AJ, 101, 865
Racine, R., & Harris, W. E. 1992, AJ, 104, 1068
Rich, R. M., Mighell, K. J., Freedman, W. L., & Neill, J. D. 1996, AJ, 111, 768
Schilbach, E., Kharchenko, N. V., Piskunov, A. E., Röser, S., & Scholz, R.-D. 2006, A&A, 456, 523
Sérsic, J.-L. 1968, Atlas de Galaxias Australes (Cordoba: Observatoria Astronomico)
Spitzer, L. 1987, Dynamical Evolution of Globular Clusters (Princeton, NJ: Princeton Univ. Press)
Stanek, K. Z., & Garnavich, P. M. 1998, ApJ, 503, L131
Strader, J., Smith, G. H., Larsen, S., Brodie, J. P., & Huchra, J. P. 2009, AJ, 138, 547
van den Bergh, S. 1994, AJ, 108, 2145
Vesperini, E. 1998, MNRAS, 299, 1019
Weidner, C., Kroupa, P., & Larsen, S. S. 2004, MNRAS, 350, 1503
Whitmore, B. C., & Schweizer, F. 1995, AJ, 109, 960
Williams, B. F., & Hodge, P. W. 2001, ApJ, 548, 190
Wilson, C. P. 1975, AJ, 80, 175
Wolff, S. C., Strom, S. E., Dror, D., & Venn, K. 2007, AJ, 133, 1092